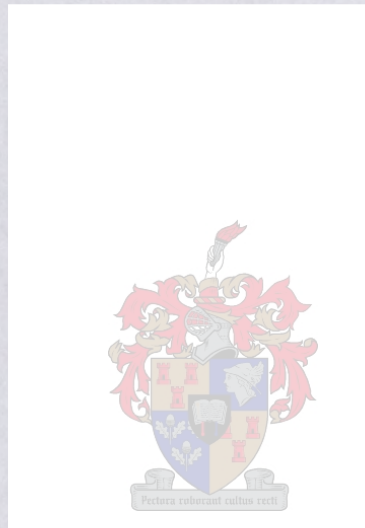# A Dual Circularly Polarized Single Element Microstrip Patch Antenna

Pamela Ruth Maki

Thesis presented in fulfillment of the requirements for the degree of
Master of Science in Engineering Science (Electronic) at Stellenbosch University

Study Leader: Professor K. D. Palmer

April 2004

DECLARATION

I, the undersigned, declare that the work contained in this study project is my own original work and has not previously in its entirety or in part been submitted at any other university for a degree.

P. R. MAKI   Date

ABSTRACT

This thesis discusses the design of a dual circularly polarized single element antenna with special emphasis on achieving a wide bandwidth and high polarization isolation. The aim of the study is to produce an antenna for transmission of colour video signals between a ground station and a low earth orbit satellite.

Microstrip patch antennas are suitable for satellite applications because they are light weight, conformal and have a thin profile. However, the antennas' inherent narrow bandwidth is one of their major drawbacks. The aperture coupled microstrip patch antenna boasts of a much-improved bandwidth over the traditional single layer microstrip antenna and the freedom of using separate substrates for the patch and the feeding network. Hence the designed single element antenna is aperture coupled. To achieve dual circular polarization with good polarization purity, the antenna had a crossed slot aperture with a balanced feed. The feed network was designed on a single layer.

The design was executed in two steps using IE3D moment of methods simulation software: design of the radiating part, and design of the feed part. Each part was simulated and optimized on its own before the two were combined, simulated and optimized again. Parameters used in the antenna optimization were: the substrates' thicknesses and dielectric constants, patch and aperture dimensions, and the feed line width and offset.

The designed antenna was built and measured. Initial measurements of S-parameters yielded unacceptable results, especially for S_{22} and S_{21}, and so an investigation into the matter was conducted. That led to the sizes of the feed and reflector planes being extended. Absorbing material was used between the parallel feed and reflector planes because some power was, to a lesser extent, still escaping, due to the fact that the planes were finite.

Measurement results demonstrated reasonable agreement with the simulation. The final antenna had a reflection coefficient of less than -10 dB for the entire operating band of 400 MHz centred on 3 GHz, an isolation of approximately -15 dB in the operating band and a gain of 2 dBi and 1 dBi for Ports 1 and 2, respectively, at 3 GHz. These results, especially the gain, are influenced by the back radiation and the finite sizes of the feed and reflector planes. It is therefore recommended that an enclosed cavity be used at the back of the antenna and a 'dogbone' aperture be used to minimize back radiation.

OPSOMMING

Die tesis omskryf die ontwerp van 'n tweevoudige sikuler gepolariseerde enkel-element antenne met spesiale klem op wye bandwydte en hoe polariserings isolasie. Die doel van hierdie studie is om 'n antenne vir uitsending van kleur video seine tussen 'n grond stasie en 'n omnentelingsatelliet daar te stel.

Mikrostrook plakantennes is gepas vir satelliet toepassings weens hulle ligte gewig en dun profiel. Die antenne se gepaardgaande nou bandwydte is egter een van hulle grootste nadele. Die gleufgekoppelde mikrostrook plakantenne gee egter 'n baie beter bandwydte as die tradisionele enkellaag mikrostrook plakantenne asook die vryheid om verskillende substrate vir die plak en die voernetwerkte gebruik. Vir hierdie redes daar besluit om die enkel-element antenne sleufgekoppeld te maak. Om tweevoudige sikuler gepolariseerde met goeie polarisasie suiwerheid te kry, moes 'n kruisvormige gleuf met 'n gebalanseerde voer ontwerp word. Die voernetwerk was op 'n enkellaag ontwerp.

Die ontwerp was in twee fases in IE3D momentmetode simulasie sagteware gedoen: ontwerp van die stralings gedeelte, en ontwerp van die voer gedeelte. Elke gedeelte word afsonderlik gesimuleer en geoptimiseer voordat die twee saam gesimuleer en geoptimiseer word. Parameters wat gebruik word in die antenne optimiseering is: dikte van substraat en dielektriese konstante, plak en gleuf grootes, en voer lynwydte en afwyking.

Die ontwerpde antenne is gebou en gemeet. Aanvanklike metings van S-parameters het onaanvaarbare resultate gelewer, veral vir S_{22} en S_{21}, dus is daar besluit om die redes daarvoor te ondersoek. Dit het daartoe gelei dat die voer- en reflector vlakte groter gemmak is. Absorbeer material is tussen die parallel voer- en reflector vlakke gebruik aangesien steeds drywing verloor is weens die eindige vlakke.

Meting resultate het taamlike goed met die simulasies vertoon. Die finale antenne het 'n weerkaatskoeffisient laer as -10 dB getoon vir die volle bandwydte van 400 MHz gesentreerd rondom 3 GHz, 'n isolasie van ongeveer –15 dB in die bandwydte en 'n aanwins van 2 dBi en 1 dBi vir onderskeidelik Poorte 1 en 2 by 3 GHz. Hierdie resultate veral die aanwins is deur die straling na agter beinvloed en die eindige grootes van die voer- en reflector vlakke. Dit word om hierdie rede dus voorgestel dat 'n geslote holte aan die rugkant van die antenne gebruik word en dat 'n "dogbone" gleuf gebruik word om straling na agter te minimeer.

ACKNOWLEDGEMENTS

I should like to thank the following for their contributions:

My study leader, Professor K. D. Palmer and Wessel van Brakel

for their guidance and support;

SED personnel for the manufacture of antennas;

Friends and acquaintances who offered their moral support;

The Department of Communications for financial assistance;

My relatives for their moral/financial support;

My children Makhi, Qaqamba and Azile for their love, support and patience;

And, most of all, God Almighty for carrying me through and for the wisdom bestowed on me.

TABLE OF CONTENTS

LIST OF FIGURES

1 INTRODUCTION

1.1 Introduction and specifications

This report covers the design of a suitable antenna for transmission of video signals to a ground station from a low earth orbit (LEO) satellite such as SUNSAT, which was developed in the Department of Electrical and Electronic Engineering at Stellenbosch University.

As LEO satellites are only visible for a few hours a day, and even less than an hour, a whole day's video information that is recorded in the satellite must be sent during this period. This means that the bandwidth requirement of the antennas is 10 to 20 times higher than for normal video, and typically is 50 MHz. Due to the use of multiple bands in these communication channels, a much wider bandwidth is often specified. For the design presented here, the bandwidth requirement is taken as 400 MHz. This will be the $S_{11} < -10$ dB target value. The system centre frequency is arbitrarily selected as 3 GHz, due to the availability of in-house support for manufacture and testing of antennas at this frequency.

The antenna under consideration is intended as the satellite antenna and physical mounting considerations limit the size to having to fit on the satellite base plate. A patch antenna would be ideal. This size limitation of approximately 10 cm x 10 cm will be shown later in this report to have serious repercussions for the practicality of the design. The size of the antenna will limit the attainable gain:

$$G = \left(\frac{4\pi A_e}{\lambda^2} \right)$$ 1.1

to approximately 8 dBi, A_e is the effective area of the antenna and λ is the wavelength. The planar nature of the satellite base means that a patch antenna would be suitable, although an ordinary microstrip patch antenna has a narrow bandwidth. It must also be borne in mind that the surface of the satellite base is not entirely available for use by the antenna; it has to serve other functions of the satellite, like providing an unobstructed view for the camera.

Due to the unpredictable nature of the relative satellite orientation, a circularly polarized antenna is required since if the two communicating antennas were linearly polarized the ground station antenna would have to be constantly adjusted to be aligned with the satellite antenna. To add to the potential operational bandwidth, it was further decided that both left and right hand circular polarization should be supported with isolation between two orthogonal antenna ports. The isolation requirement is high in practice but difficult to obtain over a wide band. A target value of -20 dB was assumed. The antenna specifications are summarized in Table 1.1.

Table 1.1: Specifications

Centre frequency	3 GHz
BW	400 MHz
S_{11}/S_{22}	< -10 dB
Size	0.1 x 0.1 m^2
Gain	Approximately 8 dBi
Polarization	Dual circular
Cross polarization	-15.34 dB (3 dB axial ratio)
S_{12} isolation between ports	-20 dB
Construction	Patch antenna with radome

To meet these specifications, a decision was taken to implement a single element antenna, which is a two-port aperture coupled microstrip patch antenna (ACMPA). The ACMPA was chosen because of its polarization purity, bandwidth, compactness and because it conforms to the structure that bears it.

1.2   Literature study

A review of literature has shown that surprisingly little reported research has been done on dual circular polarization of patch antennas with only one element. This is probably because of the complicated feed geometry required of such an antenna. Only two applicable papers, by E. Aloni and R. Kastener [1] and J. R. Sanford and A. Tengs [2], could be found.

A recent paper by A. E. Fathy, L. S. Napoli, E. Delinger, F. McGinty, D. McGee, G. Ayers, and C. E. Rodeffer [3] has proposed an interesting dual circular feed for a patch array and the design in this report is based on a novel adaptation of this to the single element case.

1.3   Thesis layout

Chapter 2 deals with the design technique and the proposed structure for the two-port antenna is discussed. Chapter 3 discusses the implementation of the antenna and initial measurement results and error determination are reported. Chapter 4 reports on the final measurement results and compares them to the specifications and simulation results. Chapter 5, the conclusion summarizes the whole thesis.

2 DESIGN

2.1 Introduction

In Chapter 1, a single element antenna with a two-port ACMPA providing for both left and right hand circular polarization with isolation between two orthogonal antenna ports was recommended. This chapter focuses on the design of the recommended antenna topology.

2.2 Proposed structure

The feed networks for single element patch antennas with dual circular polarization used in the cited literature all have their problems: [1] used serial feeding resulting in asymmetry, but in this research parallel feeding was used to overcome the problem; [2] used an additional substrate so that the feed networks for the two polarizations were on separate substrates, which was chosen because this leads to a simpler feed structure than when the whole feed network for the two polarizations are on the same substrate. This research has opted for the feed on one substrate. [3] achieved dual circular polarization with the use of a single substrate for the network; however, this was applied to an array and not a single element. The design by [3] is adapted in this research to produce dual circular polarization in a single element.

2.2.1 Fathy et al.'s design of a 2x2 dual circularly polarized array

Fathy et al. [3] adopted sequential rotation to obtain dual circular polarization in a four-element array by transposition of a diagonal pair of elements, which results in switching of the hand of polarization. They developed a six-port feed network (Figure 1) comprising two input ports (1 and 2) and four output ports (3 to 6) to feed an array of linearly polarized (LP) elements (Figure 2). A pair of quadrature hybrid circuits provides proper phasing for the discrimination between orthogonal modes.

One input to each of the hybrid couplers was connected to Port 1 and the other to Port 2 so that one port was RHCP while the other was LHCP [4, p 64 - 73]. This follows from the fact that each input terminal of a 3-dB hybrid coupler yields an opposite sense of polarization. Each hybrid coupler further has two output ports with equal amplitudes and a 90° rotational phase. The two pairs of output ports of the hybrids became the output ports for the network (Ports 3 to 6) of Figure 1.
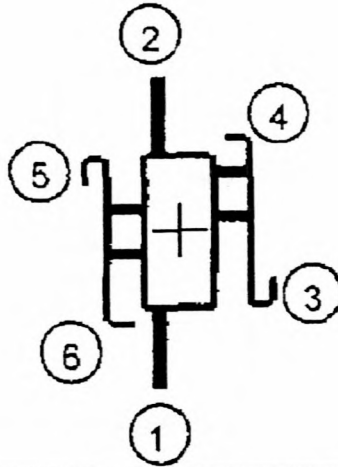
Figure 1: Planar polarizer - Six-port network for dual feed [3]
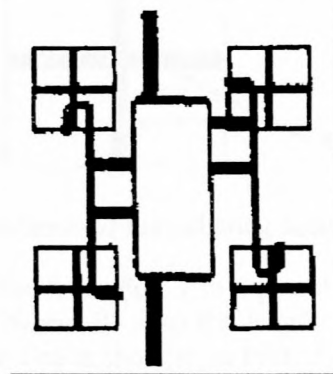
Figure 2: Feed plus four linearly polarized aperture coupled elements [3]

2.2.2 Proposed structure for the single patch dual circularly polarized antenna

The novel planar polarizer six-port circuit for dual circular polarization that was designed by [3] was adapted to a single patch antenna in this research. This adaptation uses the feed layer consisting of a six-port planar circuit with two input ports (1 and 2) connecting to the power source and four output ports (3 to 6) connecting to the four arms of a crossed slot of a single patch. One input port provided LHCP, the other RHCP. As part of the six-port planar circuit, the two quadrature hybrid couplers were connected in such a way that proper phasing, resulting in discrimination between the orthogonal modes, was achieved. To prevent overlapping of the networks from the two inputs, one of the hybrid couplers, as shown in Figure 3, was twisted. Figure 3 is a sketch of the proposed feed network, while Figure 4 is the sketch of the radiating section of the antenna consisting of a crossed slot aperture and a patch radiator on different heights in the antenna. The four output ports in Figure 3 feed the four arms of the crossed slot in Figure 4.
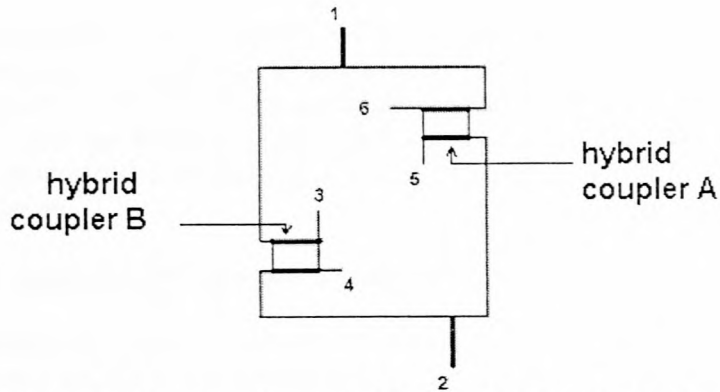
Figure 3: Schematic diagram of proposed six-port feed for single element antenna
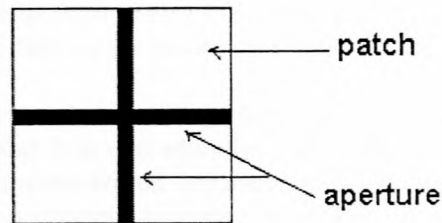
Figure 4: Schematic representation of the radiating section of the proposed structure

The length of the transmission line from Port 1 to input of hybrid A is $\lambda/2$ shorter than the length from Port 1 to input of hybrid B. Also the lengths of the transmission lines at the outputs are such that at Port 4 the line is shortest; at Ports 5 and 6 the lines are equal but they are both $\lambda/4$ longer than at port 4; at Port 3 the transmission line is $\lambda/2$ longer than at Port 4. Suppose port 2 is terminated and port 1 is driven, then at centre frequency, relative phases at output ports are: $0°$ at Port 6; $-90°$ at Port 5; $-180°$ at Port 4 and $-270°$ at Port 3 and the amplitudes at ports 3 to 6 are equal and are half the amplitude at Port 1. Both the input impedance and isolation bandwidth are broad since a 3dB hybrid has a broadband nature.

2.2.3 Polarization purity and feed symmetry

The crossed slot aperture coupled patch radiating structure in Figure 4 was chosen to deliver good polarization purity. To achieve circular polarization, a square patch was used to excite the TM_{10} and the TM_{01} modes. The two orthogonal modes were excited with equal amplitudes and in phase quadrature. Both dual and circularly polarized antennas require good isolation between the two modes. As good polarization purity is a function of the patch quality and the feeding structure, the quality of polarization is dependent on excitation of the two orthogonal modes.

Circular polarization is achieved in typical aperture coupled patch antennas by using either two off-centre apertures or a cross-shaped aperture. The use of two off-centre apertures results in an inherent asymmetry in the antenna, thereby diminishing the level of circular polarization purity [5, p. 214]. For the cross-shaped aperture, the feed network crosses the

2-3

four arms of the aperture at four coupling points. The coupling points must be geometrically symmetric, whilst being fed with equal amplitudes and a 90° rotational phase. In this way the crossed slot aperture is symmetrical and balanced providing good axial ratio purity. It was noted earlier that Aloni and Kastner [1] have used a crossed slot but the coupling points were fed serially with progressively attenuating power that resulted in asymmetry in the radiation and poor port isolation.

2.2.4   Aperture coupled microstrip patch antenna

Figure 5 is a diagram of a linearly polarized ACMPA and is presented here to show the structure of a typical ACMPA. Microwave energy is coupled from the feed circuitry to the patch radiator through coupling slots. For the linearly polarized antenna a single rectangular slot is used and the feed is simply a transmission line feeding across the centre of the slot. The slot interrupts current in the ground plane. This generates an E-field in the slot. The generated E-field couples to the E-field of the patch.

The ACMPA, by virtue of its structure, has a large bandwidth, high gain, good mechanical characteristics, and low weight and it is cost-effective [6, p. 207]. It is multi-layered; as a result the radiating patch and the feed are on separate layers, since their requirements are different. It is required of the patch substrate to have a thick, low dielectric-constant substrate for purposes of large bandwidth, but the feed may use a thin, high dielectric-constant substrate. The large bandwidth of this antenna can also be explained by the fact that the aperture acts as a second resonator in combination with the patch antenna, where the two have slightly different resonant frequencies to achieve a larger bandwidth [5, p. 215]. Foam is often used for the patch substrate because it has low permittivity that is close to 1. Metal patches cannot be deposited directly onto the foam and are therefore deposited on the underside of a dielectric material which also acts as the radome. A large aperture contributes to the enhancement of the bandwidth, but the back radiation from the aperture is a limiting factor. A large aperture is also desirable for obtaining the necessary coupling to match the impedance of the antenna. The reflector shown in Figure 5 is added to eliminate the back radiation.
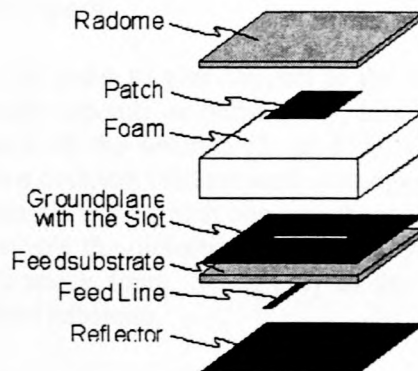
Radome
Patch
Foam
Groundplane
with the Slot
Feedsubstrate
Feed Line
Reflector

Figure 5: A linearly polarized aperture coupled patch antenna [7]

2.3   Design technique

The design detail is divided into two designs; one for the feed network and the other for the aperture slots and radiating patch. Simulation software is a necessary part of modern antenna design.

2.3.1   The simulation software

The design tool that was used is the moment of methods IE3D simulation software [8], which is a full-wave solution capable of analyzing multi-layer configurations. IE3D is used to predict the behaviour of the antenna, yielding results such as radiation pattern, input impedance, reflection coefficient and field calculations. The predicted results lead the designer to an optimum design, and are compared with measurements after the antenna has been constructed. IE3D does have a few disadvantages, though.

- It does not consider connectors, which join the antenna to the measuring instrument via a coaxial cable.
- It normally assumes an infinite ground plane and infinite dielectric layers [9, p. 125] and yet the antenna that is constructed is made to have a finite ground plane and dielectric layers, implying that the modelled structure is not identical to the actual structure, therefore the predictions may differ from the measurements.
- A large structure is demanding on computer resources and requires a long time for running the simulation.

In spite of all these disadvantages, IE3D yields a good prediction for the antenna performance.

2.3.2   Design of the radiating section

In designing an ACMPA, it is imperative to specify the substrates in terms of thickness and dielectric constant, as well as patch and aperture dimensions and the feed line width and offset. The following two subsections discuss this.

2.3.2.1 Choice of dielectric layers

Dielectric materials are used in order to give support to the metallic layers of the antenna. Selection of dielectric materials depends on permittivity, loss and thermal stability, as these factors affect the performance of the antenna [5, p. 373]. Cost is also considered when selecting the materials; hence a compact feed network is designed to save materials. There are many types of dielectric materials from which one can choose when an antenna is designed. Here choice is based on what role the dielectric materials play. Inexpensive GML 1000 was used as the radome [10], Ecostock foam, SH-2, [11] as the patch substrate and low loss RT/duroid 6002 [12] as the feed substrate.

One function of a radome is to give an antenna protection from the environment without interfering with the radiated energy. It is necessary for the radome to be included with the antenna during the design stage to avoid detuning of the patch with the radome being added

afterwards. GML 1000 is not necessarily space qualified, as needed in the application, but it is chosen for the prototype due to availability and cost constraints.

The height should not be so high as to compromise coupling of the patch to the aperture, or so low as to limit the bandwidth. 10 mm was found to be a good compromise between too high and too low (This was determined in IE3D with the complete design of the radiating section). Ecostock SH-2 was used for the patch substrate.

The feed substrate is chosen to be thin for good coupling between the feed and the aperture, as well as to minimize surface waves [13]. The RT/duroid 6002 material is used as it has low losses.

With the substrates chosen, the patch and slot sizes had to be designed.

2.3.2.2 Determination of antenna input impedance

The first approximation of the patch length was determined, using equation 2.1 [5, p. 6-14]:

$$L \cong 0.5 \times \frac{\lambda_0}{\sqrt{\varepsilon_r}} \qquad\qquad \textbf{2.1}$$

where λ_0 is the free-space wavelength and $\varepsilon_r = 1.04$, the permittivity of the patch substrate. A rectangular microstrip patch antenna, shown in Figure 6, essentially consists of a half-wavelength microstrip line to ensure that the two edges radiate in phase. This open-ended transmission line is a resonator, whose fringing field, shown in Figure 7, is the source for the antenna radiation.
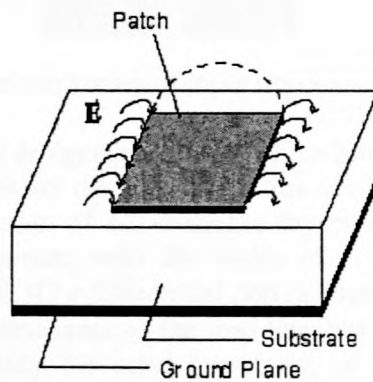

Figure 6: Typical microstrip patch antenna [7]

Figure 7: Cross-section through the substrate [7]

The aperture, which was made from two perpendicular rectangular slots, was cut in the ground plane, which is between the feed substrate and the patch substrate. The length of each slot was made equal to the length of the patch and the width of each slot was approximately one tenth of its length [13]. For symmetry, the patch was centred over the aperture. A reflecting surface was placed at 10 mm away from the feed layer (Figure 5). Each slot was fed with a pair of coupled ports (+1 and -1; +2 and -2) that are 180° out of phase in order to account for the phase reversal caused by the oppositely directed feed lines at the two feed points for each slot, resulting in two ports and four feed points with phases 0°, -90°, -180° and -270°. The ports were attached to small sections of the feed between the bottom air layer and the feed substrate. Figure 8 shows the three layers with feed sections, aperture and radiating patch.
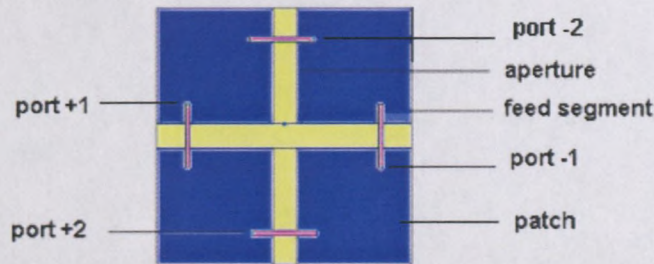
Figure 8: Geometry for determination of input impedance of radiating section in IE3D

Executing the design starts by designing the width of the four feed lines. IE3D simulation was used to determine the widths of the feed lines that correspond to specific characteristic impedances, with the properties of all dielectric layers included. A 70 Ω characteristic impedance feed line was chosen, with the width of 1.10 mm is a practical value for manufacturing. Note that in IE3D a differential port is used, so that a port reference level of 140 Ω, which is double the impedance of the feed line, has to be specified in the simulation. The port impedance is actually the input impedance of the antenna. When the targeted antenna impedance was known, determination of the dimensions of the aperture and patch to yield the necessary input impedance was performed using simulation.

Sullivan and Schaubert [14, p. 977], in their analysis of a linearly polarized ACMPA, described how the antenna can be designed to have a specific input impedance. The aperture length can be adjusted to obtain the desired resistive part of the impedance and the open-circuited stub length or overhang can be adjusted to obtain the desired reactance. In our case, where circular polarization was considered (Figure 8) and the rectangular slots were equal in

length to the patch, the input impedance was found to be a function of the separation between the two coupling points of each rectangular slot, the feed overhang as well as the width of the aperture. To obtain the resistive part of the impedance, the separation between the two coupling points was adjusted, as well as the width of the aperture. Just as in the case of the linearly polarized ACMPA, the feed overhang was adjusted to obtain the desired reactance. Positioning the feed line towards the edge of the slot reduces the coupling but it might be necessary for the sake of achieving the desired antenna impedance.

The final design was arrived at by simulation and iteration in IE3D. The results of a convergence test for adequate meshing is shown in Figure 9, with cell sizes of $\lambda/20$ being adequately converged.
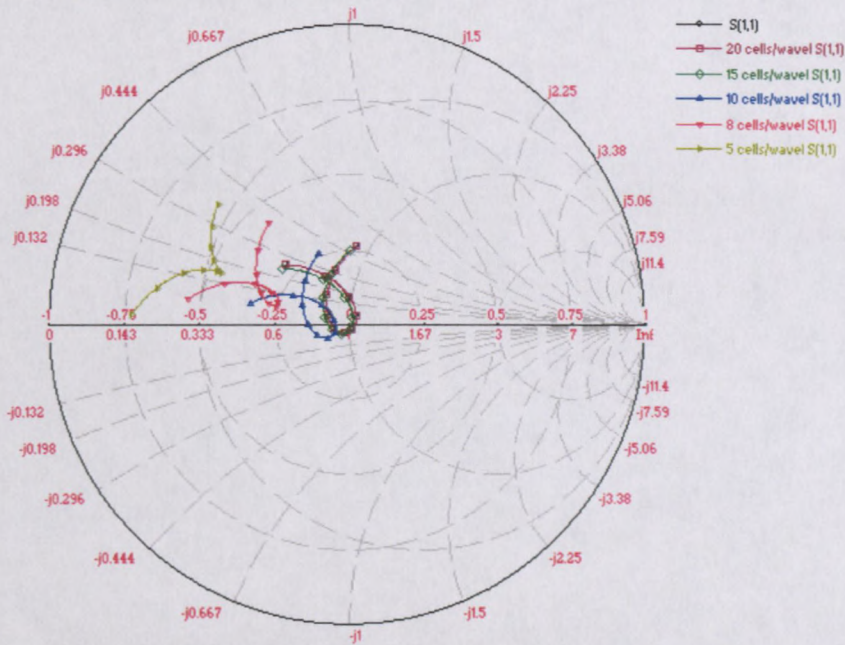
Figure 9: S_{11} convergence test results for frequencies 2.5 GHz to 3.5 GHz

Table 2.1: Dimensions for parameters of radiating section

Description	Label in figure	Length in mm
Patch length	a	64
Width of feed line	b	1.1
Separation between two feed sections	c	47.36
Feed overhang	d	4.9
Width of aperture	e	6

The values of the dimensions that are given in Table 2.1 correspond to Figure 10. The final simulation results for the geometry in Figure 10 are shown in Figure 11 and Figure 12, where both the graph of the reflection coefficient and the Smith chart show good impedance

matching for an input impedance of 140 Ω over a broad band. Table 2.2 gives substrate parameters for the complete design.
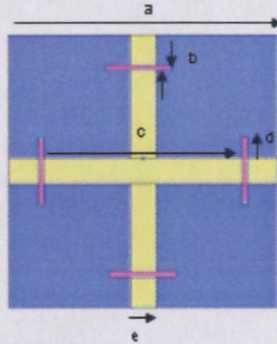
Figure 10: Radiating section of final geometry in IE3D

Table 2.2: Substrate parameters for the complete design

Name of substrate	Parameter	Value
GML 1000	Thickness	1.524 mm
	Permittivity	3.05
	Loss factor	0.003
Ecostock SH-2	Thickness	10 mm
	Permittivity	1.04
	Loss factor	0.001
RT/duroid 6002	Thickness	0.762 mm
	Permittivity	2.94
	Loss factor	0.0012
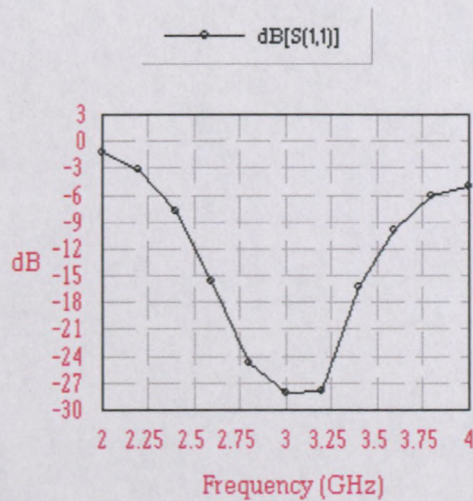
Figure 11: Computed graph of reflection coefficient for Port 1 of radiating section

2-9
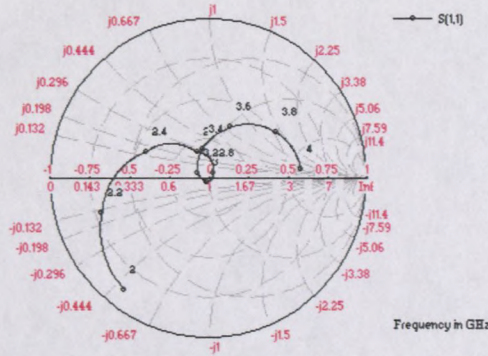
Figure 12: Computed graph of input impedance of Port 1 of radiating section

2.3.3 Design of the feed part

As discussed, the feed network is required for delivering power to the radiating structure. The feed network should match the 50 Ω ports 1 and 2 with the four coupling ports, delivering equal power and a 90° phase shift to each. Ports 1 and 2 should deliver opposite sense of rotation for the phase. Figure 3 shows schematically how the feed was implemented, while Figure 13 shows the actual geometry.
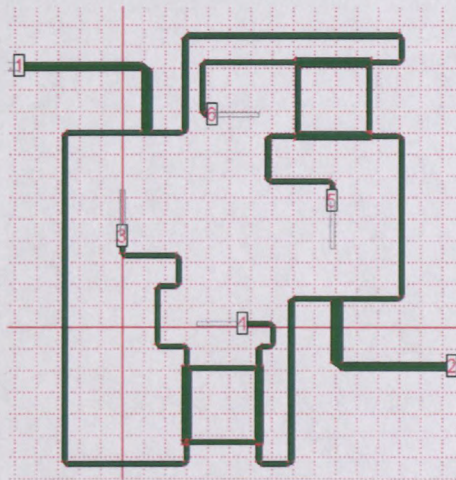
Figure 13: The designed six-port feed network

The discussion of the feed section starts with the design of a hybrid coupler since this has to be designed first, and then two hybrid couplers are joined both to the coupling points and to the signal source via the main transmission line, 70 Ω, of the feed network. Operation of the feed network as a whole will be discussed thereafter.

A 3-dB quadrature branch line coupler is made by two main transmission lines shunt-connected by two secondary transmission lines, effectively providing four quarter-wavelength transmission lines connected together in a square format [15, p. 159]. The two main

transmission lines are each Z_0 and the two secondary lines' characteristic impedances are each [16, p. 379-383]

$$Z_s = Z_0 \Big/ \sqrt{2} \qquad\qquad \mathbf{2.2}$$

where $Z_0 = 70\ \Omega$ and $Z_s = 49.5\ \Omega$. The geometry of the 3-dB quadrature branch line coupler is shown in Figure 14. The 3-dB quadrature branch line coupler has four ports, having a 90° phase difference between the two output ports, ports 2 and 3, named through and coupled arms.
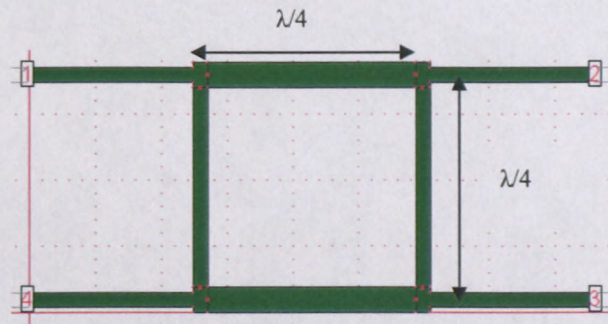
Figure 14: A 3-dB quadrature hybrid coupler

For the branch line coupler to function ideally at the centre frequency, it has to satisfy two conditions. Firstly, S_{11} and S_{14} have to be equal to zero, thus the four-port network will be perfectly matched looking into Port 1, and Port 4 is isolated. Secondly, magnitudes of S_{12} and S_{13} have to be equal, with a 90° phase difference. Each port has an identical environment, with two lines of different input impedance branching from it. Each input terminal, Ports 1 and 4, gives an opposite sense of circular polarization. The geometry is simulated and optimized so that it yields the necessary matching conditions, which are demonstrated in the simulation results of Figure 15 and Table 2.3.

Figure 15: Computed S-parameters for the 3-dB hybrid coupler

Table 2.3: Data from simulation of the 3-dB coupler

Zc(1)=(70, 0) Ohms, Zc(2)=(70, 0) Ohms, Zc(3)=(70, 0) Ohms, Zc(4)=(70, 0) Ohms, Mag(Sij) in no unit and Ang(Sij) in degree.

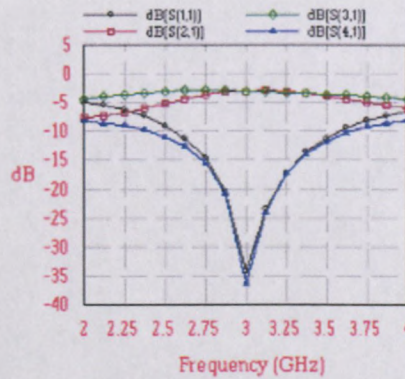| Freq[GHz]	Mag[S(1,1)]	Mag[S(2,1)]	Ang[S(2,1)]	Mag[S(3,1)]	Ang[S(3,1)]	Mag[S(4,1)]
2	0.5561	0.4078	-143.9	0.6	160.5	0.3858
2.125	0.523	0.4263	-150.4	0.6243	146.7	0.3712
2.25	0.4781	0.4555	-157.5	0.6491	132.4	0.351
2.375	0.42	0.4958	-165.8	0.6724	117.5	0.3224
2.5	0.3488	0.5445	-175.7	0.6909	102	0.2827
2.625	0.2673	0.5961	172.6	0.702	86.26	0.2303
2.75	0.1806	0.643	159.3	0.7046	70.48	0.1658
2.875	9.49e-002	0.6784	145	0.7002	54.97	9.243e-002
3	1.899e-002	0.6981	130.2	0.6918	39.87	1.49e-002
3.125	6.516e-002	0.7012	115.4	0.6828	25.12	6.224e-002
3.25	0.1359	0.6891	100.8	0.6742	10.55	0.1349
3.375	0.2041	0.6647	86.83	0.6658	-3.973	0.2003
3.5	0.2696	0.6319	73.64	0.6563	-18.5	0.2567
3.625	0.3305	0.5947	61.42	0.6446	-33	0.3034
3.75	0.3846	0.5572	50.23	0.6303	-47.35	0.3409
3.875	0.4306	0.5224	40.06	0.6143	-61.43	0.3698
4	0.4703	0.4925	30.82	0.5984	-75.26	0.3916

Operation of the feed network can be described with the help of Figure 16 and Figure 17. A signal comes in at Port 1. It goes through AB, the 50 Ω line and is transformed by BC (42 Ω) to 35 Ω at C, where the two parallel 70 Ω transmission lines, CD and CI, meet. D and I are input points of the two hybrid couplers for Port 1 where I is $\lambda/2$ later than D. The signal entering D goes through the hybrid coupler to E and F, the output ports of the coupler, where F is a $\lambda/4$ later than E. The signal thereafter travels over two equal lengths, EG and FH, both 70 Ω, in such a way that H is $\lambda/4$ later than G. The path from I to the two coupling points, L and M is identical to the one from D to the two coupling points, H and G, therefore they are fed in a similar manner. Effectively, G is fed at 0°, H at -90°, M at -180° and L at -270°. Feeding the aperture in this way makes Port 1 to be LHCP. Port 2 operates in a similar manner as Port 1, but with an opposite rotation and the two ports are isolated. Detailed geometry is given in a file in the appended stiffy disk (file: feedscale.dwg).
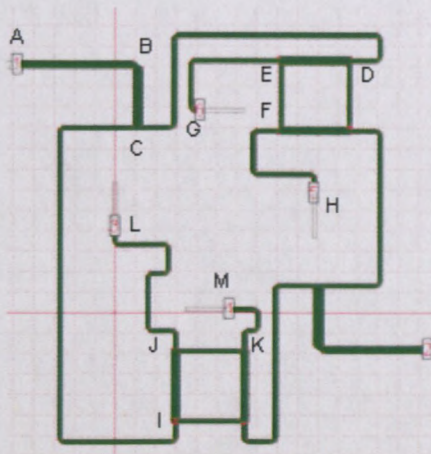

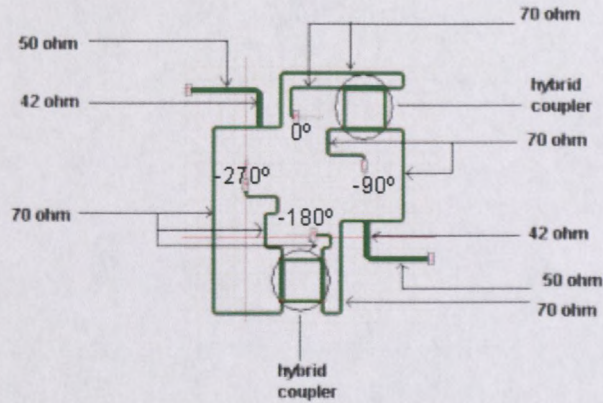Figure 16: Feed network showing path of signal for Port 1

Figure 17: The feed network showing details of transmission lines

The full feed network in Figure 13 was simulated with each of ports 3 to 6 terminated with a 70 Ω load. Figure 18 shows the resulting port S-parameters. The reflection coefficients, S_{11} and S_{22}, show that the feed network is resonant at approximately 3.05 GHz. In the frequency band 2.8 GHz to 3.2 GHz, S_{21} is less than -30 dB.
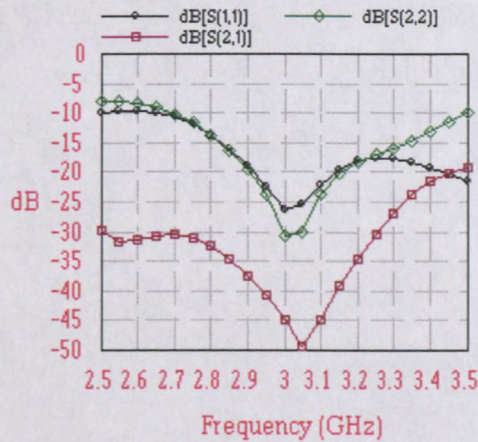
Figure 18: Port S-parameters for the full six-port feed network

2.4   Combination of radiating and feed sections

The radiating and the feed sections (Figure 19) were combined and simulated. The aim was to have the whole structure resonant at the desired operating frequency, which is 3 GHz. While a perfect match can be obtained for at a single frequency, limitations are encountered when matching over a frequency band. Simulation results (Figure 20) show that the antenna is resonant at 3 GHz for both ports. The two ports are isolated by at least 20 dB for the frequency band 2.8 GHz to 3.2 GHz.
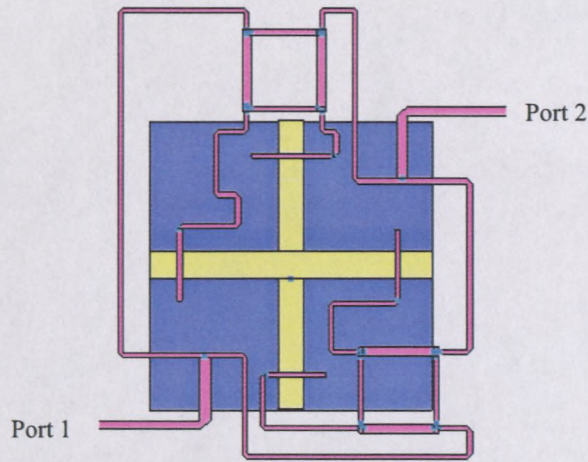
Figure 19: The full dual circularly polarized single element ACMPA
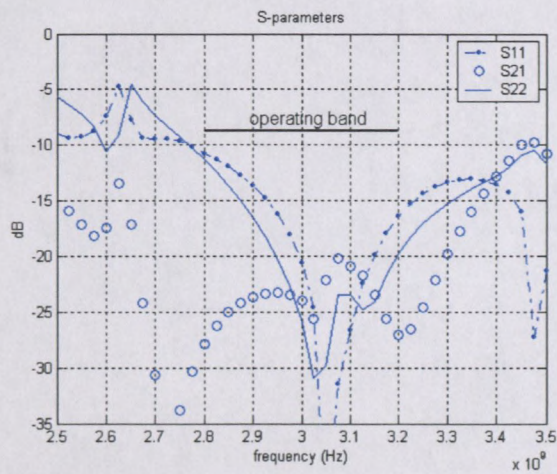
Figure 20: Computed S-parameters of the full dual CP antenna

Simulation results yielded gain and axial ratio, as well, for the complete dual circularly polarized single element antenna. A CP gain of approximately 9.2 dB was predicted for each of Ports 1 and 2 at 3 GHz (Figure 21 and Figure 22). The gain was 8.8 dBi or more for the operating band in each case. Port 1 had an axial ratio (AR) of approximately 1.5 dB on boresight at 3 GHz and Port 2 an AR of approximately 1 dB (Figure 22).

2-14
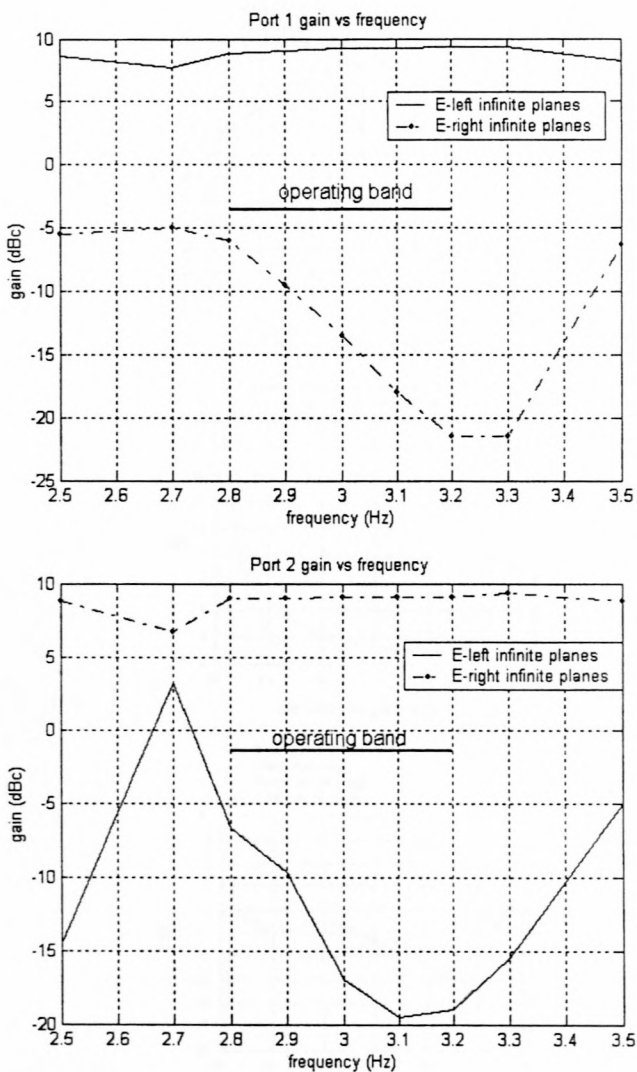
Figure 21: Computed CP gains for Port 1 and Port 2
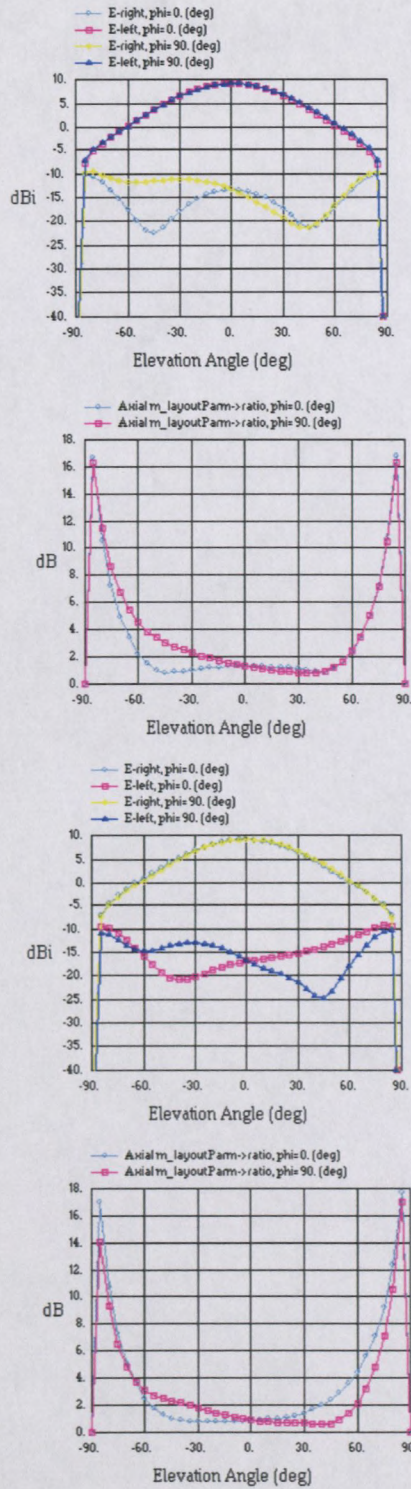
Figure 22: Computed radiation patterns and axial ratios at 3 GHz for Ports 1 and 2

2.5   Conclusion

A two-port antenna that supports dual circular polarization with good polarization purity has been designed using an aperture coupled antenna where the feed network is an adaptation of a design by [3]. The isolation between the two ports is poorer when the two sections are combined than when the feed alone is match-terminated. The predicted gain is more than target value. The performance of the antenna is satisfactory, since the target values in the specifications have been obtained.

3 INITIAL MEASUREMENTS AND ERROR DETERMINATION

3.1 Introduction

The antenna designed in Chapter 2 was built using photolithography and the dielectric materials as chosen. Figure 23 shows the antenna, whose dimensions are 10 cm x 12 cm. The radiating patch on the underside of the radome and the feed plane with the aperture are shown side by side in Figure 24. Figure 25 shows the feed network that is on the underside of the feed plane, put side by side with the radiating patch.
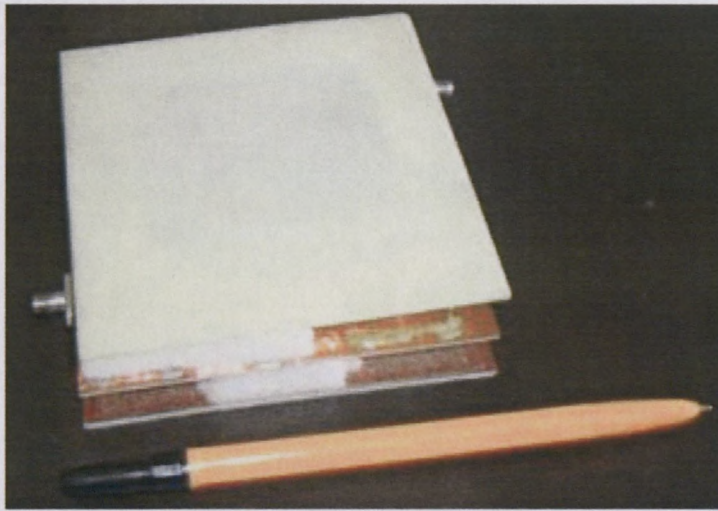
Figure 23: Picture of complete dual CP aperture coupled antenna
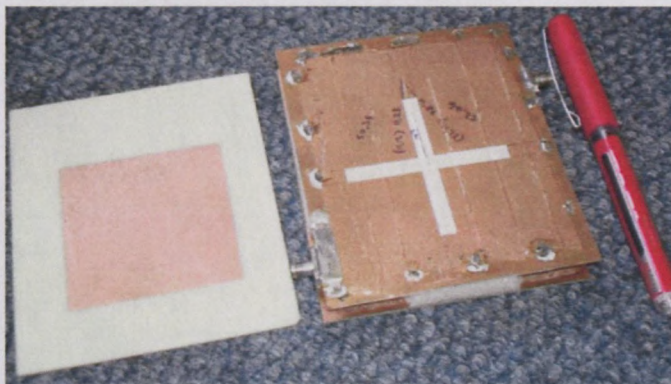
Figure 24: Picture of patch radiator and aperture
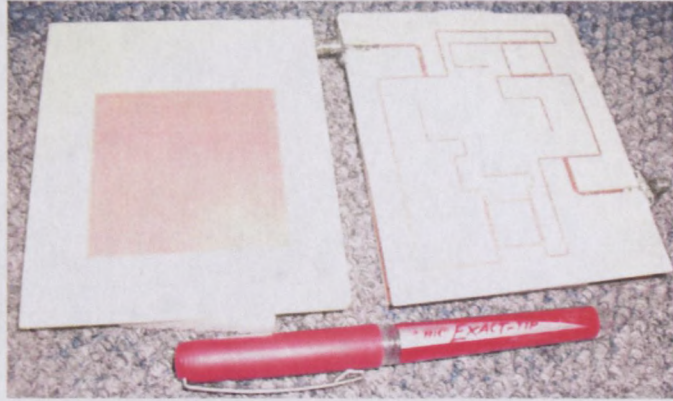
Figure 25: Picture of patch radiator and the feed layer

S-parameter measurements were taken for comparison with simulations where input impedance at both ports and isolation between the two ports were determined. The network analyzer, HP 8510C (Figure 26), was used for measurements. Measurements were taken in step mode over the frequency range 2.5 GHz to 3.5 GHz with 201 points and averaging of 64. Full 2-port calibration was performed using the 'skripsie calkit'. Calibration was verified by checking whether the electrical delay of the 'open' standard compared well with the established value.

Figure 26: The HP 8510C network analyzer that was used

3.2   Initial S-parameter measured results

The S-parameters of the antenna in Figure 23 were measured. Figure 27 shows the measured results, together with the computed results from Chapter 2. The results show unacceptable measured performance of S_{22} and S_{21} especially, and an investigation was undertaken to find the source of the error.
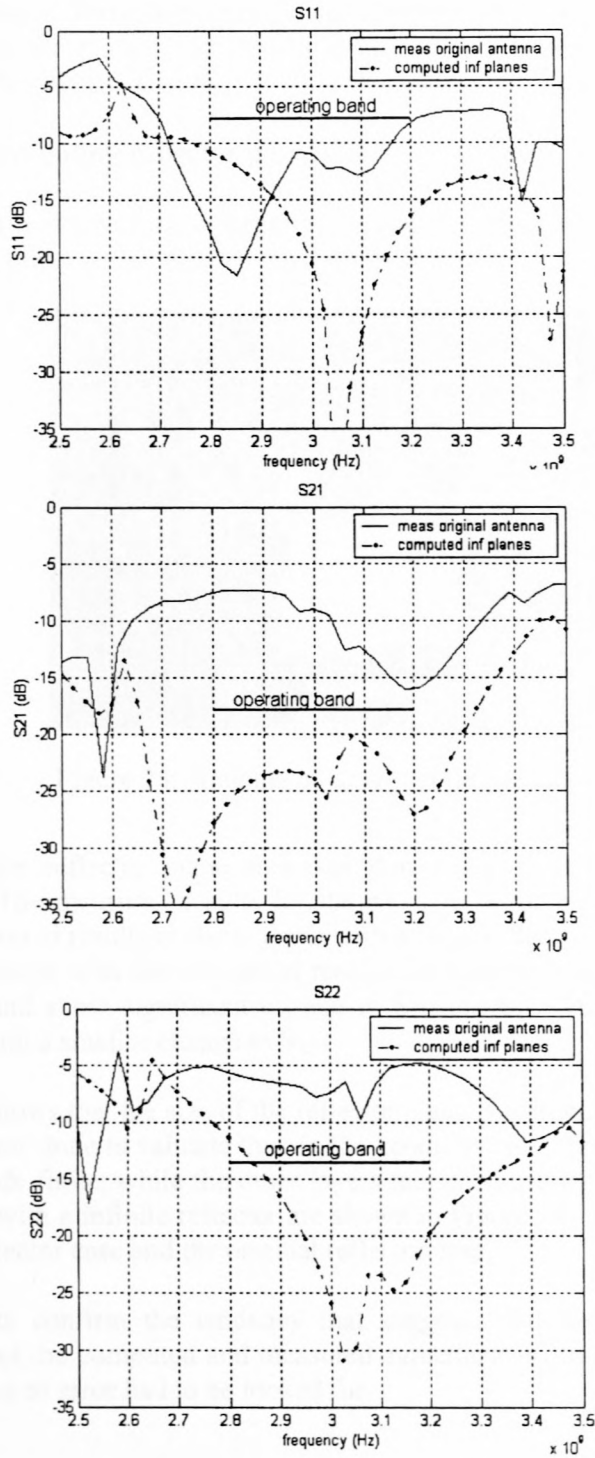
Figure 27: S-parameters of the original antenna

A fundamental difference between the computed and measured antenna geometry is the size of the conducting planes. Two conducting planes are present; the one associated with the feed (called feed plane in the report) and the one acting as a reflector to inhibit back radiation (called reflector in the report). The investigation was conducted in two steps.

- **Step 1: Investigating reflector plane size**

    The reflector plane was made larger by placing the original antenna (10 cm x 12 cm) on a circular plane with radius 40 cm. Figure 28 shows the setup.

Figure 28: Antenna on a large reflector plane

Increasing the reflector plane size was done first, as it was the easiest step to implement. The measured results for the small reflector plane antenna of Figure 23 and the measured results of the antenna with a large reflector (Figure 28) are shown in Figure 29, along with the computed results for infinite planes. The results over the operating band show significant change in S_{11} and S_{21}, when the reflector plane is increased, with a smaller change in S_{22}.

This result shows that the size of the reflector plane is a crucial parameter. A computer simulation was done to validate this. In the geometry for simulation the reflector plane size was made finite, while the other layers remained the same. Computed results for the antenna with a infinite reflector are shown in Figure 30, with measured results for the large reflector case and the original reflector case.

These results confirm the tendency that suggests that the reflector plane size is important, but the computed and measured agreement in Figure 30 not being good, a further source of error had to be looked for.
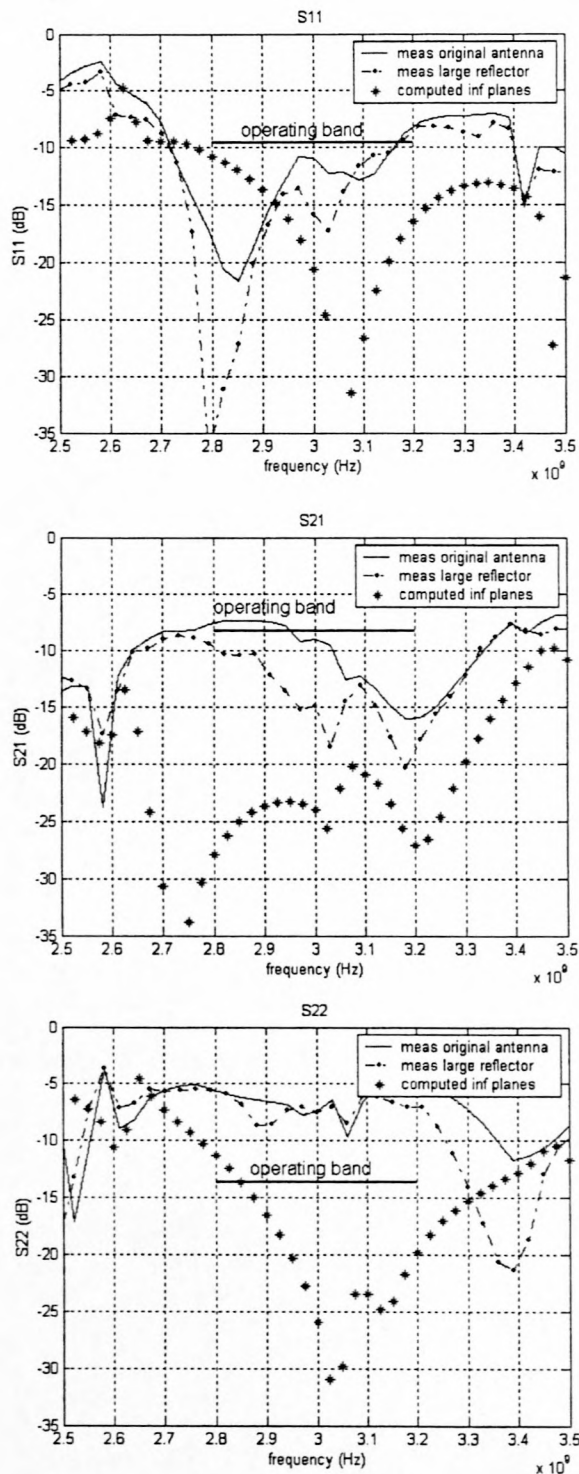
Figure 29: Measured S-parameters for small and large reflector
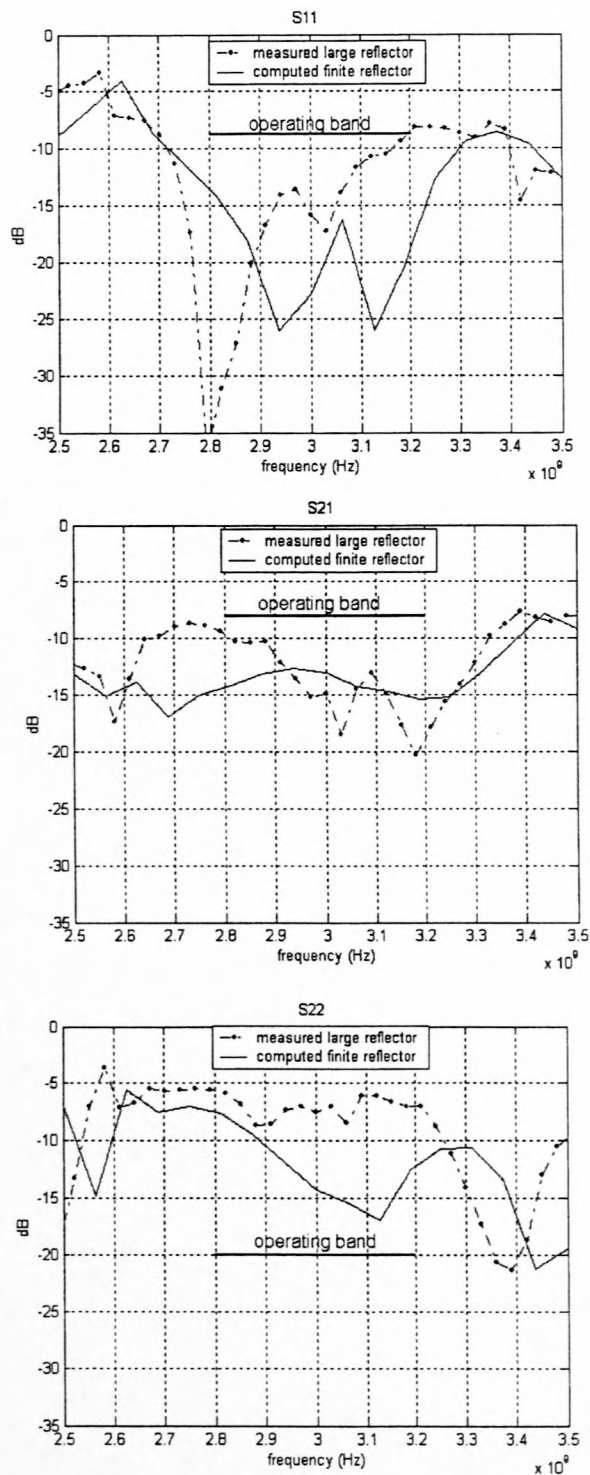
Figure 30: S-parameter computed finite reflector with measured large reflector

- **Step 2 : Investigating feed plane size**

Further experimental iterations were conducted, using absorbing material placed as shown in Figure 31 as an example. When absorbing material was placed on the reflector plane all around the antenna but not touching it, the measured S-parameters were affected. Figure 32 shows these results with and without absorbing material, as well as the computed curve for the finite reflector plane. The addition of absorbing material enhanced the performance of the antenna somewhat, especially with respect to S_{22} and S_{21}.
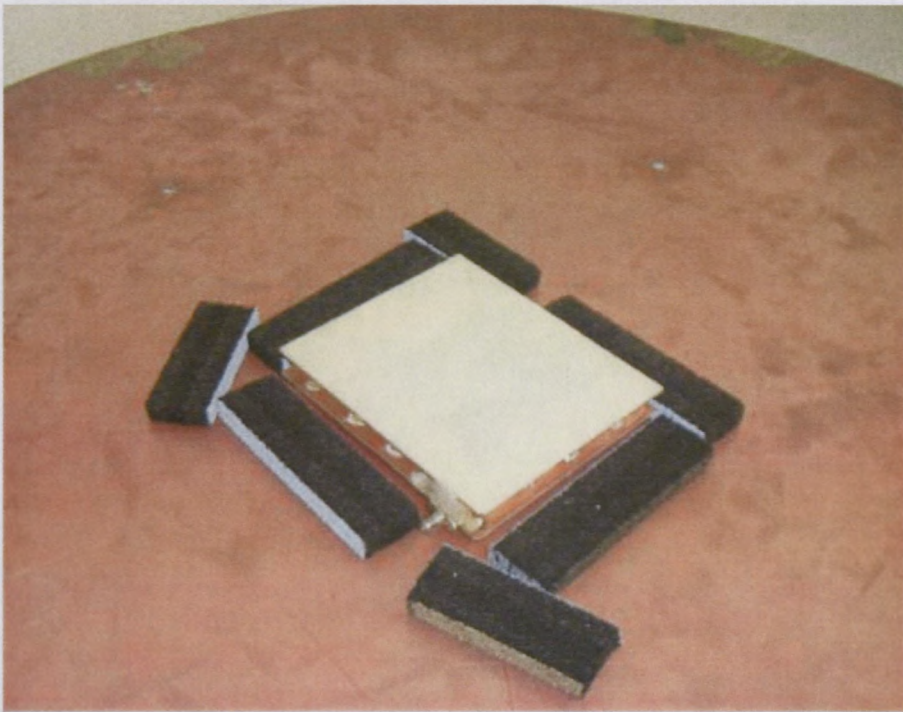
Figure 31: Antenna on a large reflector plane with absorbing material

This sensitivity to absorbing material could well occur because power is being carried between the reflector plane and the underside of the aperture or feed plane. This, together with the earlier observation concerning reflector size, led to an investigation in IE3D where sizes of both the reflector and feed planes were made finite.

Simulation results shown in Figure 33 again confirmed the observation made during measurements. This is that the performance is affected by the size of the reflector plane and that the feed plane also plays some role. It is important to note from Figure 33 that the computer simulation predicts that the isolation between ports is strongly degraded by the use of finite feed and reflector planes.
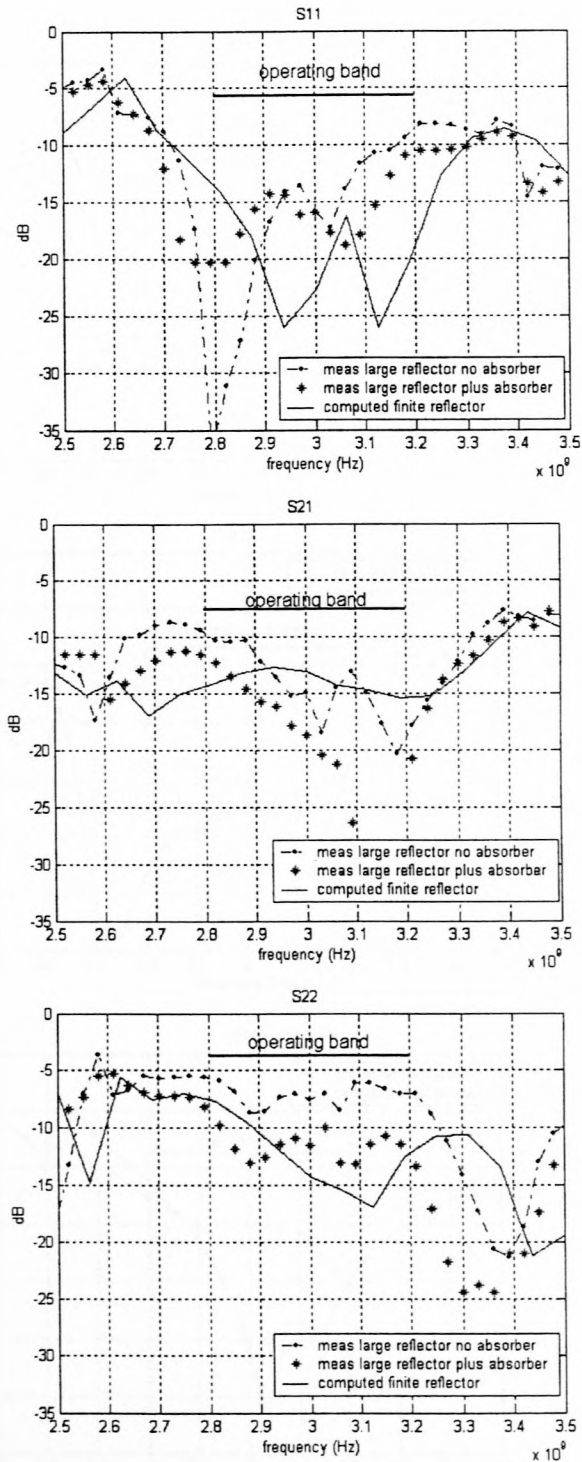
Figure 32: Measured S-parameters with and without absorbers plus computed results
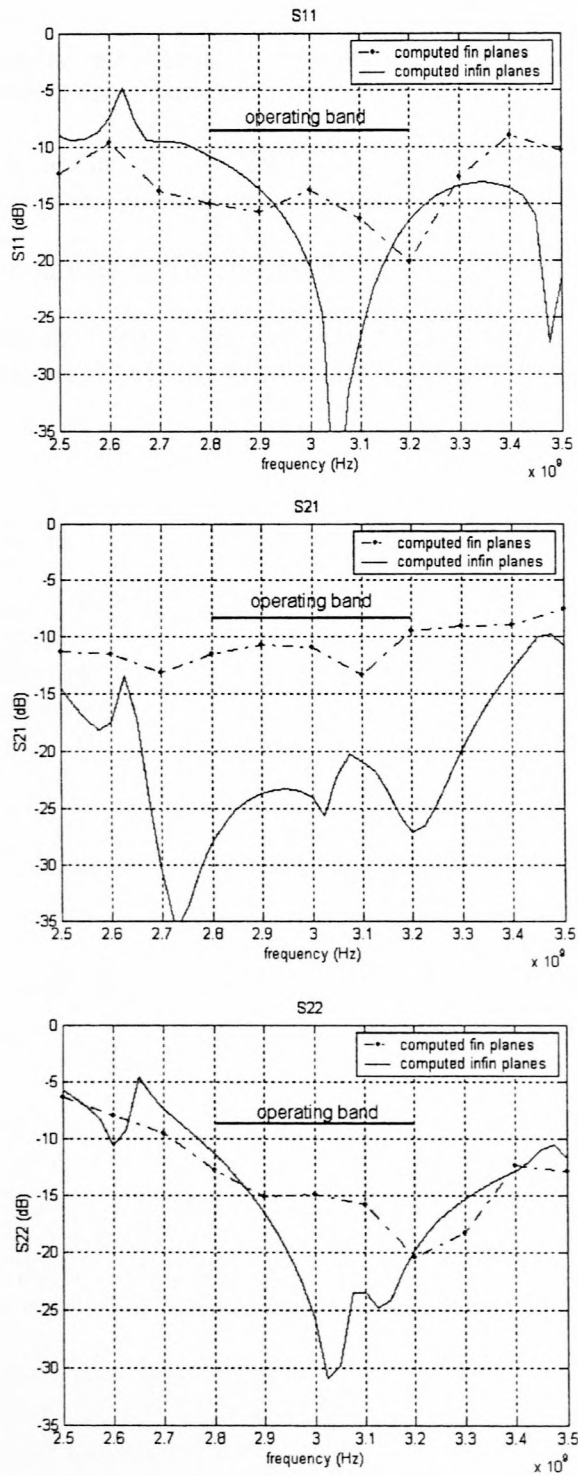
Figure 33: Computed S-parameters for finite and infinite planes

3.3   Conclusion

The differences between the initial simulation results and those that were measured indicated a wide discrepancy between the S-parameters. The errors that were identified are:

- The use of a non-infinite reflector plane to suppress back radiation caused a problem.
- Energy is propagated, probably in a parallel plate TEM mode between the two metallic planes.
- The use of a non-infinite feed or aperture plane caused a problem.

It was decided to modify the initial antenna by extending the feed plane and mounting it on a large reflector plane. The results of this operation are reported in the next chapter.

4 FINAL MEASUREMENTS AND DISCUSSION OF RESULTS

4.1 Introduction

Figure 34 shows the antenna with the extended feed plane on a large reflector, as suggested in Chapter 3. The reflector plane has a 40 cm radius and the feed plane measures 30 x 30 cm^2. The procedure for the measurement of S-parameters as described in Chapter 3 was repeated. Gain measurements were also taken.
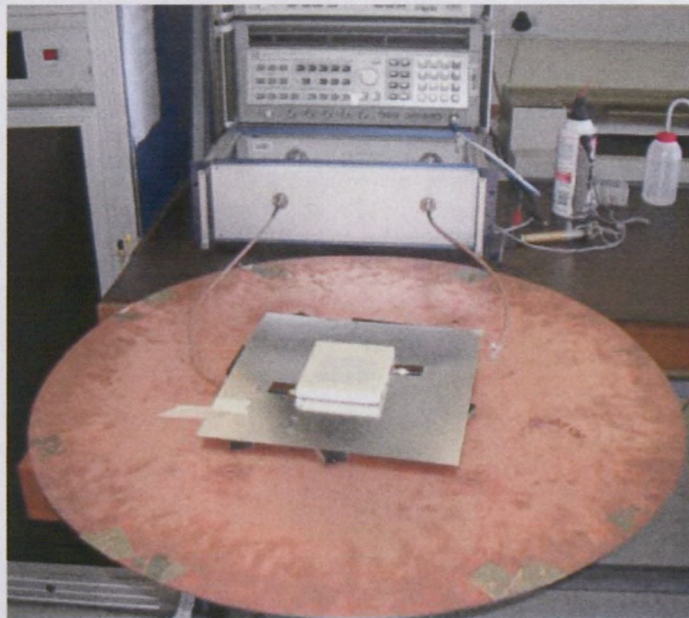
Figure 34: The final antenna configuration

4.2 Final S-parameter measured results

The final measured S-parameters are shown in Figure 35, with three graphs of S_{11}, S_{21} and S_{22}. The antenna is resonant at approximately 2.93 GHz for Port 1, and at 2.98 GHz for Port 2 with both port impedances showing passable agreement between measured and computed values. The reflection coefficient for both ports was less than -10 dB for the operating band.

The isolation between the two ports was approximately -15 dB in the operating band, which is about 10 dB poorer than predicted. The sensitivity to the feed plane size has been shown in Chapter 3, and the 10 dB difference is ascribed to this effect.
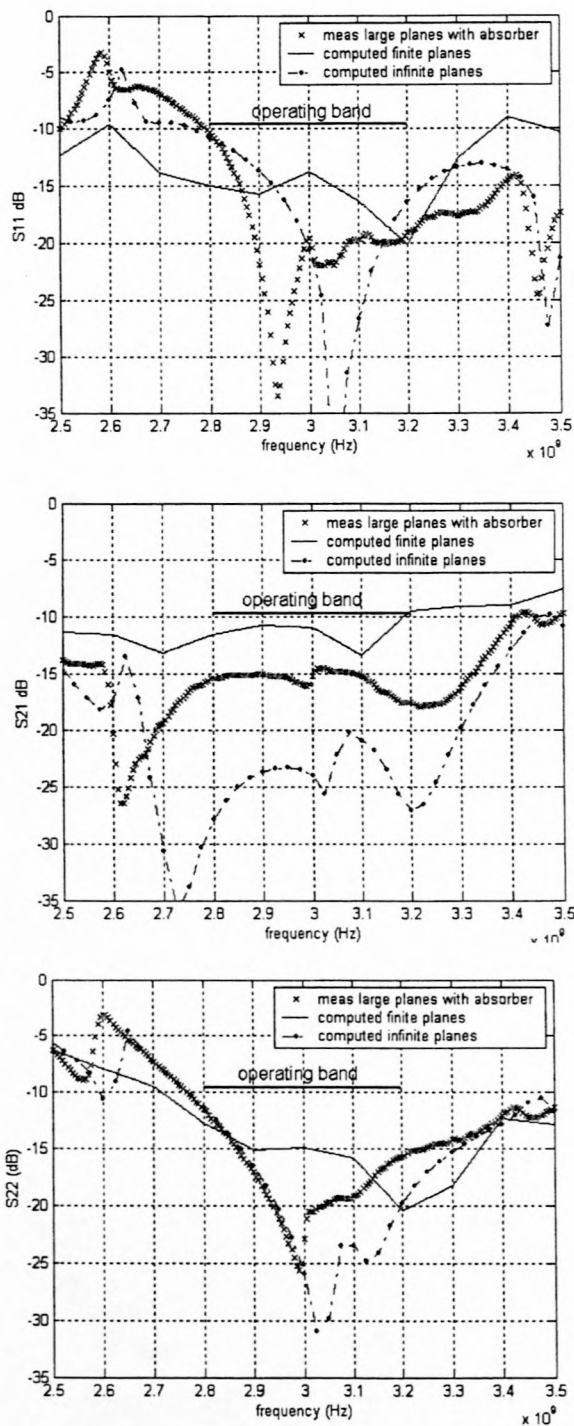
Figure 35: Final S-parameters measured and computed

4.3   Gain measurements and calculated pattern

The antenna in Figure 34 was used for measurement of gain. Gain was measured at one port at a time with the other port terminated in a 50 Ω load. The setup is shown in Figure 36. When the measurement was taken, aluminium tape was used to close the gaps (appearing as "Vs" in the aluminium in the photograph) that were cut in the feed plane for making connections to the antenna.
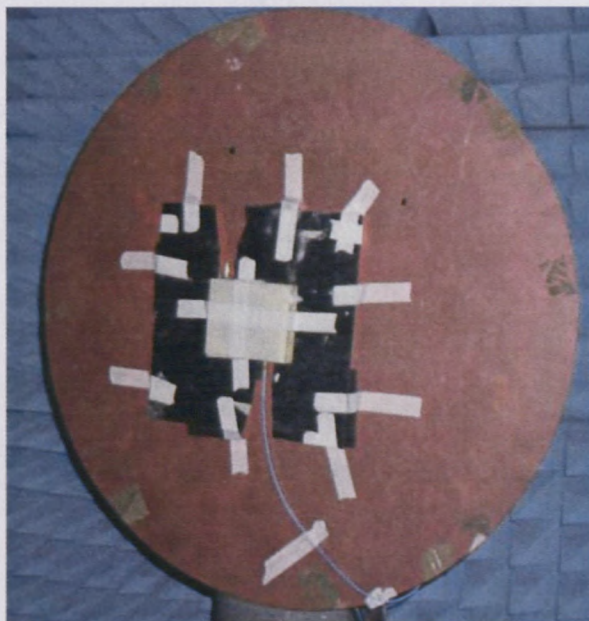
Figure 36: Final antenna as used in gain measurement in anechoic chamber

The frequency range for measurement was chosen as 2.5 GHz to 3.5 GHz with 201 measurement points. Averaging was set at 64 and a response calibration was done for which only the thru standard was used. The three antenna gain method [4, p 867 - 868] was performed with two identical linearly polarized horns and the patch antenna, with the patch transmitting and the horn receiving. Separation between the two antennas was approximately 5 m and the antennas were aligned for boresight radiation with the help of a spirit level. First S_{21} between two horns was measured. Secondly, S_{21} was measured between one horn antenna and Port 1 of the patch antenna, where the horn was oriented vertically in one instance, and horizontally for the other instance. Thirdly, a similar measurement was taken with the horn replaced by the other horn. Ports were exchanged, and measurements between horns and Port 2 of the antenna were taken in a similar fashion.

Using the Friis equation (equation 4.1) [4, p. 89], the gains of the two horns were eliminated and the gain of the patch was determined. The gain has two components for each port, namely LHCP and RHCP gains. These were derived from the vertical and horizontal measurements of S_{21} with each horn using equations 4.2 and 4.3 [17, p. 48-52], which incorporate the

polarization mismatch factor between the linearly polarized horn antennas and the circularly polarized patch antenna.

$$S_{21} = G_r \; G_t \left(\frac{\lambda}{4\pi R} \right)^2 \left(1 - |\Gamma_r|^2 \right) \left(1 - |\Gamma_t|^2 \right) |\hat{p}_t \cdot \hat{p}_r| \qquad\qquad 4.1$$

where S_{21} is the ratio of received to transmitted power; G_r = gain of the receiver; G_t = gain of the transmitter; λ = wavelength; R = separating distance; $|\Gamma_t|$ and $|\Gamma_r|$ are the magnitudes of the transmitter and receiver reflection coefficients, respectively; $|\hat{p}_t \cdot \hat{p}_r|$ is the polarization loss factor.

$$S_{21r} = \frac{S_{21x} - jS_{21y}}{\sqrt{2}} \qquad\qquad 4.2$$

$$S_{21l} = \frac{S_{21x} + jS_{21y}}{\sqrt{2}} \qquad\qquad 4.3$$

where S_{21r} and S_{21l} are the right and left components of S_{21}, S_{21x} and S_{21y} are the measured data for when the horn antenna was in the horizontal and the vertical positions. Axial ratio is also calculated from the same data, using equation 4.4.

$$r(dB) = 20 \log \left| \frac{S_{21r} + S_{21l}}{S_{21r} - S_{21l}} \right| \qquad\qquad 4.4$$

Figure 37 and Figure 38 are the CP gain and axial ratio graphs for Ports 1 and 2, respectively.

4-5
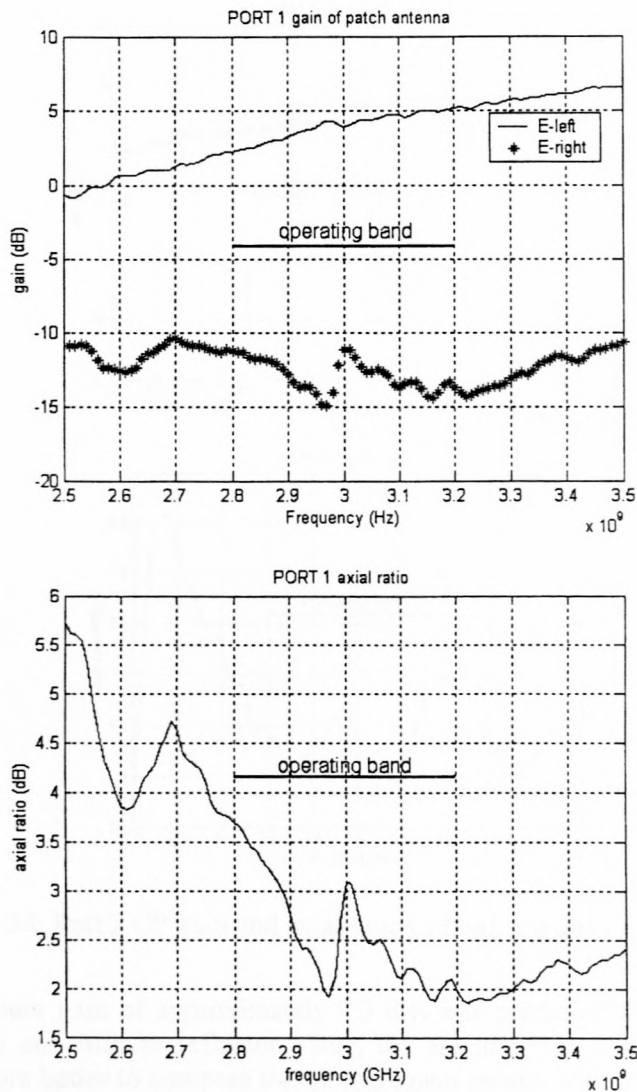
Figure 37: Port 1 CP gain and axial ratio of final antenna on boresight
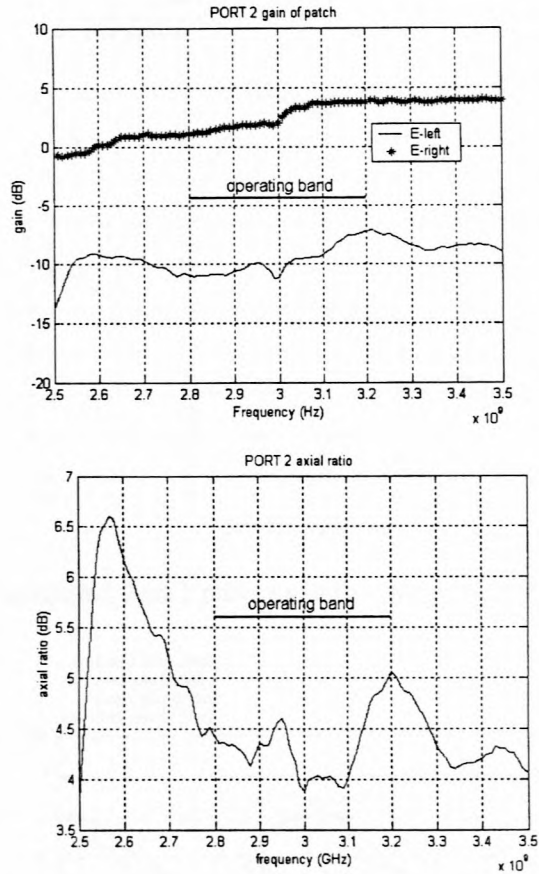
Figure 38: Port 2 CP gain and axial ratio of final antenna on boresight

Although a maximum gain of approximately 9.3 dBi was predicted for an antenna with an infinite feed plane and infinite reflector plane, the antenna that was measured had finite planes. It is therefore better to compare the measurement results with the computed results of the antenna with finite planes. There is, however, a problem with generating accurate simulations for the finite feed plane case. IE3D is readily able, at the cost of computational resources, to simulate the case of a finite reflector plane by placing a finite size conductor to be meshed. Using IE3D to simulate a finite feed plane is technically also possible, but the documentation does not recommend this. The problem is that using the only available feed model, the "vertical localized", is not recommended for microstrip lines due to diminished accuracy. However, as this was the only option, the finite case was simulated.

Accepting the limited accuracy, Figure 39 and Figure 40 show the computed patterns for the two ports on boresight at 3 GHz, while Figure 41 and Figure 42 are graphs of computed gain versus frequency. The computed antenna radiation performance using the finite feed plane is clearly substantially less than would be expected in the case of infinite planes, with the centre frequency gain dropping from 9.3 dBi to about 4 dBi.

Figure 39: Computed Port 1 patterns in the two principal planes at 3 GHz
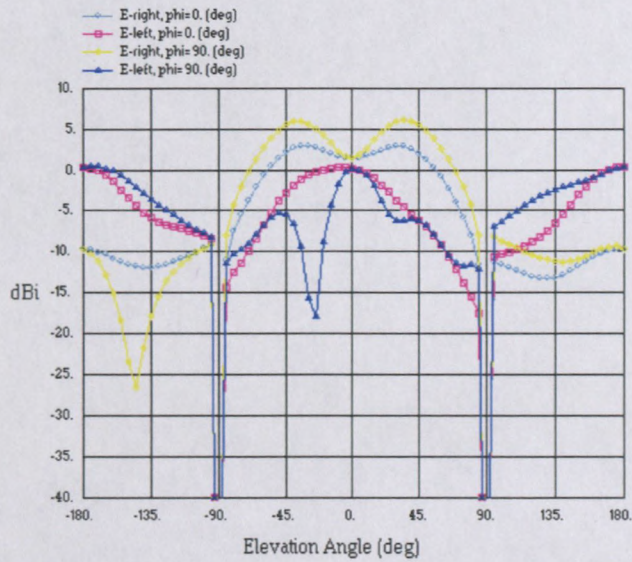
Figure 40: Computed Port 2 patterns in the two principal planes at 3 GHz

4-7
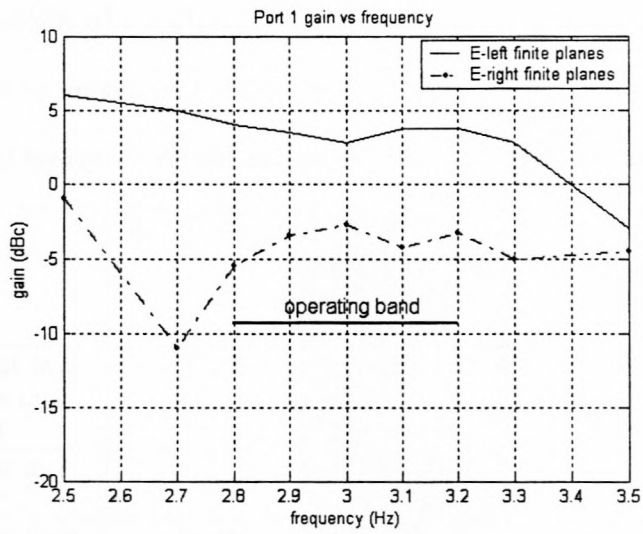
Figure 41: Computed CP gain at Port 1 of antenna with finite planes
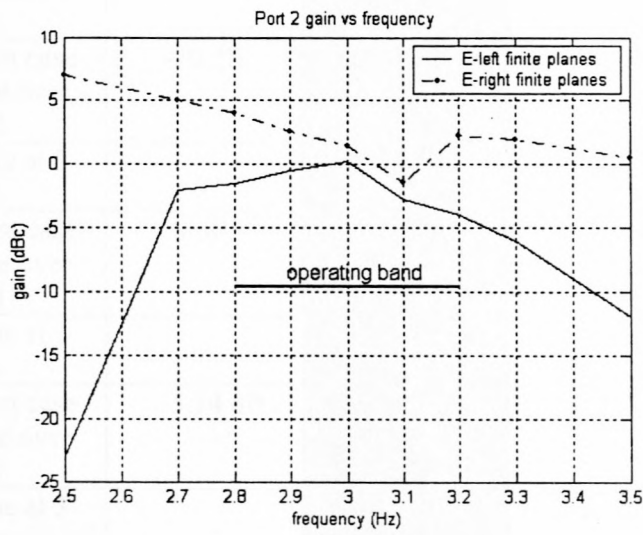
Figure 42: Computed CP gain of Port 2 of antenna with finite planes
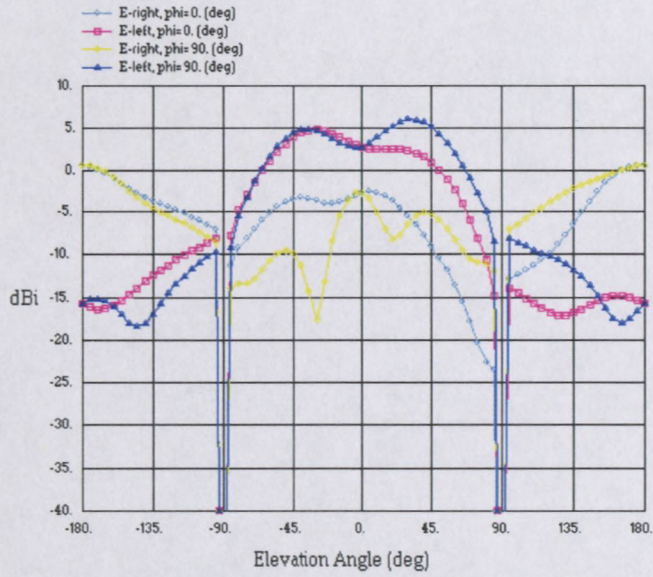
4.4 Discussion of results

The results can best be summarized in a table:

Table 4.1: Final measured results compared to specifications and computed results

		Specifications	Measured (Final antenna with extended planes)	Computed (Infinite planes)	Computed (Finite planes)
S_{11}	Worst case value over band	-10 dB	-10.5 dB	-11 dB	-14 dB
	Value at 3 GHz		-20 dB	-21 dB	-14 dB
S_{22}	Worst case value over band	-10 dB	-11.5 dB	-11.5 dB	-13 dB
	Value at 3 GHz		-25 dB	-25 dB	-15 dB
S_{21}	Worst case value over band	-20 dB	-14 dB	-20 dB	-9 dB
	Value at 3 GHz		-15 dB	-24 dB	-15 dB
Gain Port 1	Worst case value over band	8 dBi	2 dBi	8.8 dBi	3 dBi
	Value at 3 GHz		4 dBi	9.5 dBi	3 dBi
Cross polarisation Port 1	Worst case value over band	-15.34 dB	-13 dB	-15 dB	- 6 dB
	Value at 3 GHz		-15 dB	-23 dB	- 6 dB
Gain Port 2	Worst case value over band	8 dBi	1 dBi	8.8 dB	-2 dBi
	Value at 3 GHz		2 dBi	9.3 dBi	1.5 dBi
Cross polarisation Port 2	Worst case value over band	-15.34 dB	-11 dB	-19 dB	1.5 dB
	Value at 3 GHz		-13 dB	-26 dB	-2 dB

S_{11} and S_{22} of the final antenna compare well with specifications as well as prediction for an antenna with infinite planes. Isolation between the two ports of the antenna is less than required by the specifications or predicted for the antenna with infinite planes, but it is much better than predicted for the antenna with finite planes. Gain seems poor when compared to specifications and computed results for the antenna with infinite planes, but it compares well with prediction for antenna with finite planes. For Port 1, cross polarization is good, especially for frequencies higher than 2.9 GHz (Figure 37). Although the cross polarization for Port 2 does not meet the specifications (Figure 38), the performance is much better than IE3D predicts for an antenna with finite feed and reflector planes. There is no obvious explanation for the discrepancy.

A dual circularly polarized single element patch antenna was produced, although it suffers from back radiation and possibly parallel plate TEM mode. The fact that the final antenna performance differs from the predicted value is ascribed to the fact that, even though the feed plane is enlarged, it is still not infinite. The fact that the truncated feed plane continues to play a role can be seen from Figure 43, which shows how adding an absorber underneath the feed plane improves the performance by reducing reflections from the edge.

The next chapter gives an overview of the research. Successes and problems are reiterated and recommendations are mentioned.
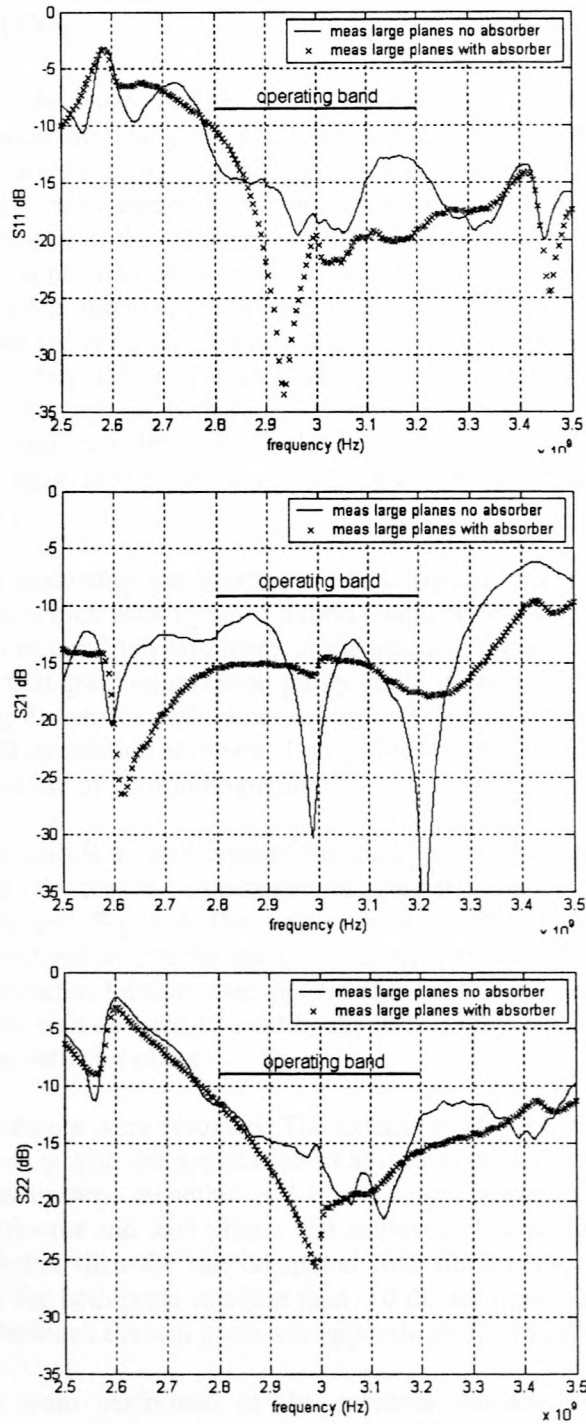
Figure 43: S-parameters showing effect of absorber on final antenna

5 CONCLUSION

The purpose of the study was to produce a dual circularly polarized single element antenna, which has a large bandwidth and good polarization purity while being compact. As such, it would be suitable for downloading large volumes of video information with high resolution in a short space of time, whilst transmitting from a satellite that is in constant motion. Target values for the performance of the antenna were set. The review of literature showed that only one of the two research papers that were found, which had dual circular polarization applied to a single element patch antenna, could operate the two polarizations simultaneously with good isolation between the two ports of the antenna. This aspect is necessary because, while it allows selection between left and right hand circular polarization, simultaneous dual polarization (not alternating or switching) provides independent coverages of the same geographical area through two electrically isolated inputs at all times. Our design sought to do the same, but by using a feed network on only one substrate instead of the two used by Sanford and Tengs [2].

An aperture coupled microstrip patch antenna was designed with an adaptation of Fathy et al.'s [3] feed network, which uses a pair of hybrid couplers on a single planar layer. Aperture coupling was used to ensure high efficiency of the antenna. Symmetry was a vital element in feeding the patch so that good polarization purity could be achieved. A process of choosing substrates and tuning dimensions of transmission lines, the radiating patch and the aperture was done, using IE3D simulation software. This yielded a satisfactory design and the antenna was produced with the use of photolithography.

The antenna that was built is a multi-layered structure, which occupies an area of 10 cm x 12 cm. S-parameters were the first to be measured and the performance of the antenna, especially the reflection coefficient S_{22} and the transmission coefficient S_{21}, was shown to be unacceptable. An investigation into the source of the error showed that the size of the reflector plane is a crucial parameter. Further investigation showed that the size of the feed plane does play some role too. It was decided to modify the antenna by extending the feed plane and mounting it on a large reflector plane.

S-parameter measurements were resumed. The extension of the planes improved the results dramatically. It was only with the application of absorbing material between the two parallel plates that the curves became smoother and a better approximation to the computed curve, which has infinite reflector and feed planes was achieved. The performance of the measured antenna was much better than the one computed with finite reflector and feed planes. The reflection coefficient for both ports was less than -10 dB for the entire operating band of 400 MHz. The isolation between the two ports was approximately -15 dB in the operating band.

Gain measurements were performed in the anechoic chamber, using the three-antenna method. When these measurements were made, one of the two ports was selected, while the other was terminated with a 50 Ω load. The measured data was processed to yield gains and axial ratios of Ports 1 and 2 on boresight. At 3 GHz the gain was 2 dBi and 1 dBi for Ports 1 and 2, respectively. Although this performance was poor when compared with specifications,

these values compare well with prediction when finite reflector and feed planes are used. In the operating band, cross polarization was more than -13 dB for Port 1 and for Port 2 it was more than -11 dB. Although these values do not meet the specifications, they are close and they are much better than the computed values for an antenna with finite reflector and feed planes.

Gain measurements and subsequent calculations cannot be accounted for properly since investigation into the causes of the discrepancies was not conducted in full. However, there seems to be some correlation between the measured gain and axial ratio and the computed gain and axial ratio when finite planes were used.

During simulation it became obvious that S_{21} is related to how well the radiating part of the antenna matches the feed part. Figure 18 which shows computed S-parameters for the feed network, shows good isolation between Ports 1 and 2 when the output ports were terminated with 70 Ω loads. When the loads were replaced with the radiating part, the isolation was significantly affected. Therefore the measured S_{21} value can be improved by tuning the impedance of the radiating part even more.

All the parameters of the antenna were influenced by the size of the reflector and feed planes. These could be improved by minimizing the back radiation, or by backing the antenna with an enclosure or both. Minimizing back radiation is achieved by making the aperture small, but this requires that the patch substrate also be thinner, thus reducing the bandwidth. Targonski and Pozar [5, p. 214] recommend the use of a 'dogbone' aperture which supports a high patch substrate while producing less back radiation than a normal rectangular aperture. Having an enclosure would cause the power to be contained, as observed with the use of absorbing material that power can be lost from underneath the feed plane.

The simplest design that satisfies the required specifications is generally the most preferable. A simpler network is generally cheaper, more reliable, and less loss-prone than a more complex design. Sanford and Tengs [2] did warn that feeding on one layer could result in a complicated feed network and their design is simpler and yields good performance.

In summary, the challenges that were presented by the high gain flat antenna, which we sought to produce, were:
- feed line losses, large bandwidth and high efficiency antenna element
- dual circular polarization with good polarization purity and high isolation

These are regarded as challenges because an ordinary microstrip patch antenna does not present them. To a large extent, they have been dealt with appropriately. With the recommendations listed above in place, especially the use of an enclosed cavity at the back of the antenna, the antenna should provide a good design. One other challenge is a compact feed. Figure 44 shows a design with improved feed compactness. The corresponding computed S-parameter curves are shown in Figure 45.
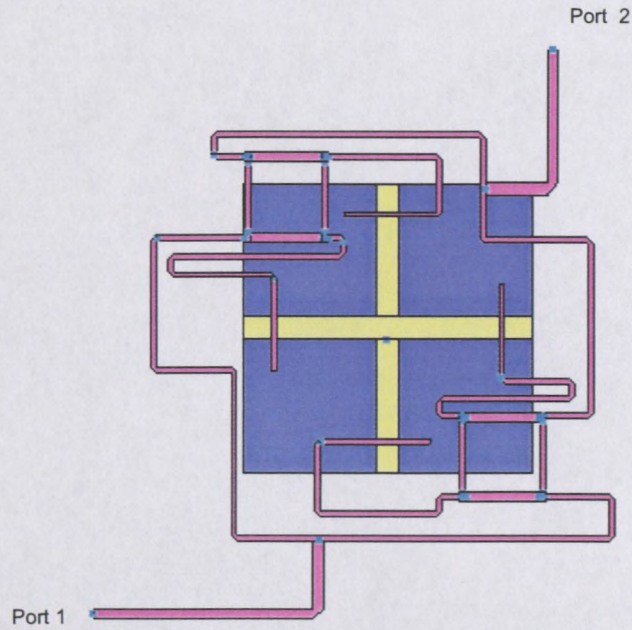
Port 2

Port 1

Figure 44: Compact geometry of a dual circularly polarized antenna

The widths of the feed network are as in Figure 19, with the detailed geometry of Figure 19 given in a file in the appended stiffy disk (file: feedscale.dwg). The aperture / patch length is 63 mm; aperture width is 5 mm and the feed overhang is 6.9 mm.
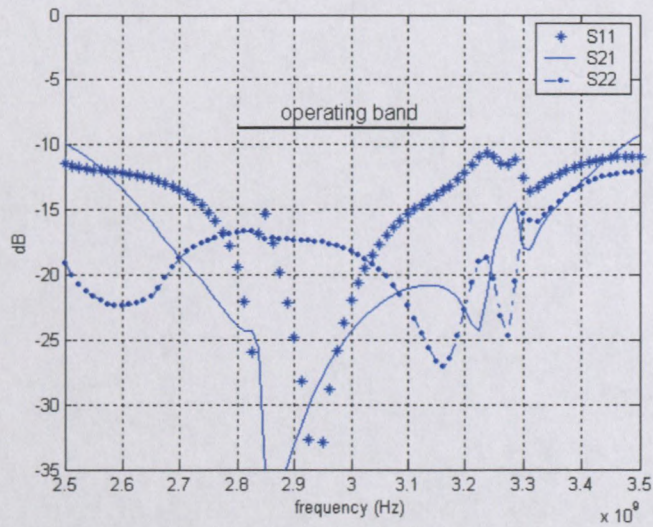
Figure 45: Computed S-parameters for the compact geometry of Figure 44

5-3

6 References

[1]   Aloni E, Kastener R. *Analysis of a Dual Circularly Polarized Microstrip Antenna Fed by Crossed Slots*. IEEE Transactions on Antennas and Propagation. August 1994; 42 (8), p 1053-1058.

[2]   Sanford J R, Tengs A. *A Two Substrate Dual Polarised Aperture Coupled Patch*. Department of Microwave Technology, Chalmers University of Technology: Gothenburg, Sweden; 1996.

[3]   Fathy A E (Sarnoff Corp.), Napoli L S, Delinger E, McGinty F, McGee D, Ayers G, Rodeffer C E. *A Novel Planar Polarizer Feed Network for Dual Circular Polarization*.   IEEE Antennas and Propagation Society, AP-S International Symposium (Digest). 2001; 3, p 412-415

[4]   Balanis C A. *Antenna Theory Analysis and Design*, 2nd edition. NY John Wiley; 1997.

[5]   Pozar D M, Schaubert D H, Editors. *Microstrip Antennas: The analysis and Design of Microstrip Antennas and Arrays*. NJ, IEEE Press; 1995.

[6]   Gardiol F. *Microstrip Circuits. NY* John Wiley; 1994.

[7]   Kuchar A. *Linear Aperture Coupled Microstrip Patch Array*. [online].[2003 01 28]; Available: http://www.nt.tuwien.ac.at.

[8]   http://www.zeland.com.

[9]   Cloete J H, Davidson D B, Palmer K D. *Microstrip Antenna Analysis and design*. Dept. E&E Engineering, University of Stellenbosch, South Africa; 1996.

[11]   http://www.gil.com

[12]   http://www.ecosorb.com

[13]   http://www.rogers-corp.com

[14]   Pozar D M. *A Review of Aperture Coupled Microstrip Antennas*. University of Massachusetts at Amherst; May 1996, p1-9.

[15]   Sullivan P L and Schaubert D H. *Analysis of an Aperture Coupled Microstrip Antenna*. IEEE Transactions on Antennas and Propagation. August 1986; AP-34 (8).

[16]   Fooks E H, Zakarevicius R A. *Microwave Engineering Using Microstrip Circuits*. NY Prentice Hall; 1990.

[17]   Pozar D, *Microwave Engineering, 2nd edition*. NY John Wiley; 1998.

[18]   Stutzman W L, Thiele G L. *Antenna Theory and Design,* 2nd edition. NY John Wiley; 1998.